



**HAL**  
open science

# Tailoring the morphology and properties of starch aerogels and cryogels via starch source and process parameter

Fangxin Zou, Tatiana Budtova

► **To cite this version:**

Fangxin Zou, Tatiana Budtova. Tailoring the morphology and properties of starch aerogels and cryogels via starch source and process parameter. *Carbohydrate Polymers*, 2020, 255. hal-03100409

**HAL Id: hal-03100409**

**<https://hal.science/hal-03100409>**

Submitted on 22 Mar 2023

**HAL** is a multi-disciplinary open access archive for the deposit and dissemination of scientific research documents, whether they are published or not. The documents may come from teaching and research institutions in France or abroad, or from public or private research centers.

L'archive ouverte pluridisciplinaire **HAL**, est destinée au dépôt et à la diffusion de documents scientifiques de niveau recherche, publiés ou non, émanant des établissements d'enseignement et de recherche français ou étrangers, des laboratoires publics ou privés.

1  
2  
3  
4  
5  
6  
7  
8  
9  
10  
11  
12  
13  
14  
15  
16  
17  
18  
19

**Tailoring the morphology and properties of starch aerogels and  
cryogels via starch source and process parameter**

Fangxin Zou, Tatiana Budtova\*

Center for Materials Forming - CEMEF, MINES ParisTech, PSL Research University, UMR CNRS  
7635, CS 10207, 06904 Sophia Antipolis, France

\* Corresponding author:  
Tatiana Budtova, [Tatiana.Budtova@mines-paristech.fr](mailto:Tatiana.Budtova@mines-paristech.fr)

20 **Abstract**

21 Porous starch materials with various morphology and properties were made via starch dissolution,  
22 retrogradation and drying either with supercritical CO<sub>2</sub> (“aerogels”) or lyophilisation (“cryogels”). Their  
23 properties were correlated with the rheological response of retrograded starch gels and crystallinity of  
24 aerogels and cryogels. All starch cryogels possess very low density (0.07 – 0.16 g/cm<sup>3</sup>), very large  
25 macropores and low specific surface area (around 3 – 13 m<sup>2</sup>/g). Their morphology is mainly the replica  
26 of sublimated ice crystals. The properties of starch aerogels strongly depend on starch source: the  
27 lowest density (around 0.1 g/cm<sup>3</sup>) and highest specific surface area (170 – 250 m<sup>2</sup>/g) was recorded for  
28 pea starch aerogels and the highest density (0.3 – 0.6 g/cm<sup>3</sup>) and lowest specific surface area (7 – 90  
29 m<sup>2</sup>/g) for waxy maize starch aerogels. The morphology and properties of starch aerogels are interpreted  
30 by amylose and amylopectin evolution during retrogradation.

31

32 Keywords: supercritical drying, freeze-drying, morphology; density; specific surface area

33

34

## 35 1. Introduction

36 Starch is one of the most abundant polysaccharides used in multiple applications: in food and non-  
37 food (biodegradable films and foams for packaging, as additive in paper and textile) and also as a source  
38 of low molecular weight chemicals. Porous starch makes a special family of lightweight materials in  
39 which pore sizes, porosity and cellular morphology depend on the processing method: for example,  
40 voids are formed during extrusion of starch/water at high temperatures, baking a starch paste followed  
41 by water evaporation, microwave heating which generates steam bubbles, freeze-drying/sublimation of  
42 ice crystals and supercritical fluid extrusion. Rather recently, supercritical fluid extraction technique,  
43 used to make aerogels, has also been applied to starch.

44 Aerogels are nanostructured lightweight mesoporous/small macropores materials with high specific  
45 surface area (of several hundreds of  $\text{m}^2/\text{g}$ ); the latter distinguishes them from foams which usually are  
46 lightweight but with very large macropores and thus low surface area. The very first aerogels were  
47 reported by Kistler in 1931 (Kistler, 1931); inorganic aerogels were then developed in the 70s-80s of the  
48 past century followed by aerogels based on synthetic polymers (Pierre, 2011). Aerogels are versatile  
49 materials: they can be used for water-oil separation (Sai et al., 2015; Zou, Peng, Fu, Zhang, & Li, 2015),  
50 thermal insulation (Groult & Budtova, 2018a; Zou et al., 2016), drug delivery (Mehling, Smirnova,  
51 Guenther, & Neubert, 2009; Ulker & Erkey, 2014) and electro-chemical/energy storage (Hamedi et al.,  
52 2013; Rooke et al., 2011) applications. In the past two decades, a variety of so-called bio-aerogels made  
53 from polysaccharides such as cellulose (Lavoine & Bergström, 2017; Budtova, 2019), pectin (Zhao,  
54 Chen, & Chen, 2017; Groult & Budtova, 2018b), starch (García-González, Uy, Alnaief, & Smirnova,  
55 2012; Zhu, 2019), and alginate (Mallepally, Bernard, Marin, Ward, & McHugh, 2013; Robitzer, David,  
56 Rochas, Renzo, & Quignard, 2008) gained widespread attention in the view of the need of sustainable  
57 and biodegradable materials on the one hand, and their potential use in biomedical applications on the  
58 other hand.

59 As most of bio-aerogels (except those based on nanocellulose), starch aerogels are made via  
60 dissolution-gelation (retrogradation for starch)-solvent exchange-drying with supercritical carbon dioxide.  
61 Starch aerogels were shown to be promising matrices for drug release (García-González et al., 2012;  
62 Mehling et al., 2009) and also for thermal insulation (Druel, Bardl, Vorweg, & Budtova, 2017). It was  
63 reported that higher starch concentration, higher aerogel density (García-González & Smirnova, 2013;  
64 Ubeyitogullari & Ciftci, 2016), as expected. It seems that higher amylose content leads to higher specific

65 surface area, for example, 200 – 250 m<sup>2</sup>/g for pea and high amylose corn (Druel et al., 2017; García-  
66 González et al., 2013) vs 20 – 80 m<sup>2</sup>/g for potato (Druel et al., 2017) and wheat starches (Ubeyitogullari  
67 et al., 2016). However, low specific surface area, 90 m<sup>2</sup>/g, was reported for high amylose starch Eurylon  
68 7 (Mehling et al., 2009), most probably because of incomplete starch dissolution. There are still several  
69 open questions such as the influence of the starch type and retrogradation time on aerogel structure  
70 and properties.

71 It should be noted that the first mention of using drying with supercritical CO<sub>2</sub> for making starch  
72 aerogels was made by Glenn *et al*, and the materials were called “microcellular foams” (Glenn & Irving,  
73 1995). This seminal work compared the structure and properties of freeze-dried and supercritically dried  
74 unmodified wheat starch, regular corn and high amylose corn starches. However, starch granule  
75 remnants were present in the dried samples and samples’ specific surface area was not measured; low-  
76 resolution scanning electron microscope (SEM) did not allow the analysis of microstructure below one  
77 micron.

78 As mentioned above, another way of making porous starch materials avoiding pores’ collapse during  
79 drying is freeze-drying. Freeze-dried starch can be used in multiple applications, mainly in food and also  
80 in biomedical area (for example, in tissue engineering). Numerous studies have been performed on  
81 freeze-dried starches, either on starch granules (B. Zhang et al., 2014), or on starch solutions alone or  
82 mixed with other natural components (Nakamatsu, Torres, Troncoso, Min-Lin, & Boccaccini, 2006;  
83 Svagan, Samir, & Berglund, 2008), or on starch emulsions (Silva, Azevedo, Cunha, Hubinger, &  
84 Meireles, 2016; Spada, Norena, Marczak, & Tessaro, 2012). In food applications, freeze-drying is  
85 considered as a way of granules’ preservation, and the influence of drying method (oven drying from  
86 water or ethanol, freeze-drying, microwave drying, etc) on starch gelatinization and digestibility was  
87 investigated (Glenn et al., 2008; B. Zhang et al., 2014). In materials science freeze-drying is used to  
88 shape the pores of starch solution (usually strong retrogradation is avoided) upon removing water  
89 (Nakamatsu et al., 2006; Svagan et al., 2008). When using starch for encapsulation, freeze-drying allows  
90 obtaining powders and is often compared with spray drying (Silva et al., 2016; Spada et al., 2012).

91 To the best of our knowledge, there is no study, except the one of Glenn *et al* (Glenn et al, 1995), on  
92 the comparison of the structure and properties of freeze-dried and supercritical dried starches made  
93 from the same starting gels. How does the way of drying and starch type (i.e. amylose/amylopectin ratio)  
94 influence starch morphology and properties? It is well documented that retrogradation kinetics depends

95 on amylose/amylopectin ratio: gelation is faster in high-amylose starches as amylose undergoes rapid  
96 recrystallization forming semi-crystalline clusters. What is the impact, if any, of retrogradation time on  
97 freeze-dried and supercritically dried starch gels? The answers to these questions will help tuning starch  
98 morphology and properties for the desired applications.

99 The goal of this work is to understand the influence of starch type (amylose content) and processing  
100 conditions (way of drying, starch concentration, retrogradation time) on the morphology and properties  
101 of porous starches starting from the same precursor. For simplicity, we will use “aerogels” for samples  
102 dried with supercritical CO<sub>2</sub>, and “cryogels” for freeze-dried samples. We correlate the morphology and  
103 properties of porous starches with their crystallinity and gel strength, and we suggest using “aerogel  
104 approach” as a way to follow starch gel structure evolution upon retrogradation and as a function of  
105 amylose content.

106

## 107 **2. Experimental**

### 108 2.1 Materials

109 Three types of starches were kindly provided by Roquette, France: waxy maize, potato and pea with  
110 amylose content around 1%, 18-21%, and 33-36%, respectively. Absolute ethanol (>99%) was  
111 purchased from Fisher Scientific. Distillated water was used. All chemicals were used without any further  
112 purification.

### 113 2.2 Preparation of starch solutions and gels

114 Starch needs to be dissolved as well as possible in order to avoid the presence of non-dissolved  
115 granules and their remnants. The residual granules and their remnants are non-porous and may  
116 decrease the specific surface areas of aerogels in a similar manner as non-dissolved cellulose fibers  
117 decreased specific surface area in cellulose aerogels (Korhonen & Budtova, 2020).

118 Different methods were adapted to dissolve the three types of starches because of their different  
119 solubility in water. Optical microscopy (LEICA DM4500P, Leica Microsystems) was used for the  
120 screening of the influence of the dissolution conditions on the presence of granules' remnants (Table  
121 S1 in the Supporting Information). The final conditions selected for each starch type were when no non-  
122 dissolved fragments were seen in optical micrographs. For example, no non-dissolved granules were  
123 detected when stirring potato starch dispersed in water at 1000 rpm at 95 °C for 2 h, but 3 h were needed  
124 to dissolve waxy maize starch in the same conditions (Table S1). To dissolve pea starch two steps

125 method (Druel et al., 2017) was used: first, pea starch-water was heated to 95 °C under stirring at 1000  
126 rpm for 1 h; then this mixture was placed in the autoclave (452HC, Parr instrument), heated during 50  
127 min up to 130 °C and kept at 130-140 °C for another 20 min under stirring at 250 rpm.

128 Starch solutions of various concentrations, from 5 to 11 wt% (in dry weight), were prepared as  
129 described above for each type of starch. Hot starch solutions were centrifuged, if needed, for 3 min  
130 under 8000 rpm to remove bubbles and poured into plastic molds. After cooling down to room  
131 temperature, all samples were stored at 4 °C for retrogradation. The retrogradation time for potato and  
132 pea starch was from 1 to 4 days and for waxy maize from 15 to 45 days. Long retrogradation times of  
133 waxy maize starch solutions were needed as in non-gelled state solution viscosity was too low not  
134 allowing making homogeneous aerogels and cryogels. In the following, starch gels are named as “starch  
135 type-Xwt%-Nday-gel”, where X is starch concentration in solution and N is retrogradation time.

### 136 2.3 Preparation of starch aerogels and cryogels

137 Starch aerogels were prepared according to the following steps: dissolution-retrogradation-solvent  
138 exchange-supercritical CO<sub>2</sub> drying. Before drying, water was replaced by ethanol through solvent  
139 exchange as water is not miscible with supercritical CO<sub>2</sub>. The solvent exchange was performed by  
140 gradual increase of ethanol in ethanol/water mixtures: first, the gels were soaked in ethanol/water 50/50  
141 (v/v) for 0.5 day, then in ethanol/water 75/25 (v/v) for another 0.5 day, and finally in pure ethanol for 3  
142 days during which fresh ethanol was exchanged twice a day.

143 Supercritical CO<sub>2</sub> drying was performed as follows. First, ethanol in the gel was slowly drained by  
144 gaseous CO<sub>2</sub> while the system was pressurized at 50 bar and 37 °C. Then, the temperature was set at  
145 37 °C, and the pressure was increased to 80 bar above CO<sub>2</sub> critical point. After that, a dynamic washing  
146 step was performed at 80 bar and 37 °C with an output of 5 kg/h of CO<sub>2</sub> for 1 h to remove the residual  
147 ethanol from the gel. It was followed by a static mode for 1-2 h under the same temperature and pressure  
148 and dynamic washing step again for 2 h. Finally, the system was kept at 37 °C and slowly depressurized  
149 to ambient conditions with pressure decrease speed 5 bar/h. Slow depressurization was used to prevent  
150 sample strong shrinkage. The autoclave was cooled down to room temperature before being opened.  
151 Starch aerogels are named as “starch type-Xwt%-Nday-aerogel” where X and N are the same as for  
152 starch gels.

153 Starch cryogels were prepared from gels using freeze drying. The gels were unidirectionally frozen  
154 by placing starch gel on a metal plate which was immersed in liquid nitrogen for 20 min, and then freeze-

155 dried for 72 h at -82 °C and pressure below 2 mTorr by using the Lyophilisateur Cryotec COSMOS-80  
156 (Cryotec). In the following, the starch cryogels are named as “starch type-Xwt%-Nday-cryogel” where X  
157 and N are the same as for starch gels.

## 158 2.4 Characterization

### 159 2.4.1 Rheology

160 The rheological properties of starch gels were probed using Gemini 150 rheometer (Bohlin  
161 Instruments) with parallel plate geometry (40 mm diameter) and gap 1000 μm. A hot starch solution was  
162 put on the lower plate, kept for 1.5 min, gap closed and the whole kept for another 3 min. Temperature  
163 was then set at 4 °C for different retrogradation times varying from 1 to 4 days before starting the  
164 oscillation. Strain response of elastic ( $G'$ ) and viscous ( $G''$ ) moduli was tested at 4 °C to determine the  
165 mechanical response of starch gels to shear strain in the range 0.1% - 1000% at frequency 1 Hz. The  
166 diameter of plates was varied to test the potential slippage; no influence of plates' geometry on  $G'$  and  
167  $G''$  values was recorded, within the experimental errors, indicating the absence of slippage.

### 168 2.4.2 Linear shrinkage

169 The total linear shrinkage of the samples due to the solvent exchange and drying was calculated  
170 according to the following equation with at least three measurements per formulation (Himmel, Gerber,  
171 Biiirger, Holzfhfiter, & Olbertz, 1995; Saliger, Heinrich, Gleissner, & Fricke, 1995):

$$172 \text{ Linear shrinkage} = \frac{D_b - D_a}{D_b} \times 100\% \quad (1)$$

173 where  $D_b$  and  $D_a$  are the diameters of sample before solvent exchange and after drying, respectively.

### 174 2.4.3 Bulk density and porosity

175 Bulk density of starch aerogels and cryogels was determined by Geopyc 1360 (Micromeritics)  
176 powder densitometer with Dryflo as the powder, with at least five measurements per formulation. The  
177 diameter of the test chamber was 19.1 mm, and the force was 25 N.

178 The porosity (%) of each sample was calculated as follows:

$$179 \text{ Porosity} = \frac{\rho_s - \rho_b}{\rho_s} \times 100\% \quad (2)$$

180 where  $\rho_b$  and  $\rho_s$  refer to the bulk and skeletal densities, respectively, with  $\rho_s = 1.45 \text{ g/cm}^3$  (García-  
181 González et al., 2013).

### 182 2.4.4 Specific surface area

183 Specific surface area ( $S_{\text{BET}}$ ) of starch aerogels and cryogels was calculated using nitrogen adsorption  
184 method with ASAP 2020 specific surface area and porosity analyzer (Micromeritics Instrument



185 Corporation). Prior to the measurement, all samples were degassed at 70 °C for 10 h. The maximal  
186 standard deviation was 12 m<sup>2</sup>/g.

#### 187 2.4.5 Scanning electron microscope

188 The morphology of starch samples was characterized by Scanning Electron Microscope (SEM)  
189 Supra40 Zeiss SEM FEG (Fields Emission Gun) (ZEISS) with an accelerating voltage of 3 kV and  
190 diaphragm 10 μm. Before the measurements, a roughly 7 nm thin layer of platinum was sputtered onto  
191 the sample's surface with Q150T coater (Quorum).

#### 192 2.4.6 X-ray diffraction analysis

193 X-ray diffraction (XRD) analysis (in reflection mode) was performed on diffractometer “XPERT-PRO”  
194 (PANalytical) with Cu K<sub>α</sub> radiation at wavelength of 1.5406 Å. The samples were grinded into powder  
195 and scanned in 2θ range from 5° to 50°. The relative crystallinity was calculated by the following equation:

$$196 \quad \text{Relative crystallinity} = \frac{A_c}{A_c + A_a} \times 100\% \quad (3)$$

197 where  $A_c$  and  $A_a$  are the integrated areas of crystalline and amorphous regions, respectively, over the  
198 2θ range from 5° to 28°.  $A_c$  and  $A_a$  were calculated using the method of Komiya and Nara (Komiya &  
199 Nara, 1986; Cheetham & Tao, 1998). Komiya & Nara showed that XRD in symmetrical reflection and  
200 symmetrical transmission modes provide almost the same values of the relative crystallinity (Komiya &  
201 Nara, 1986).

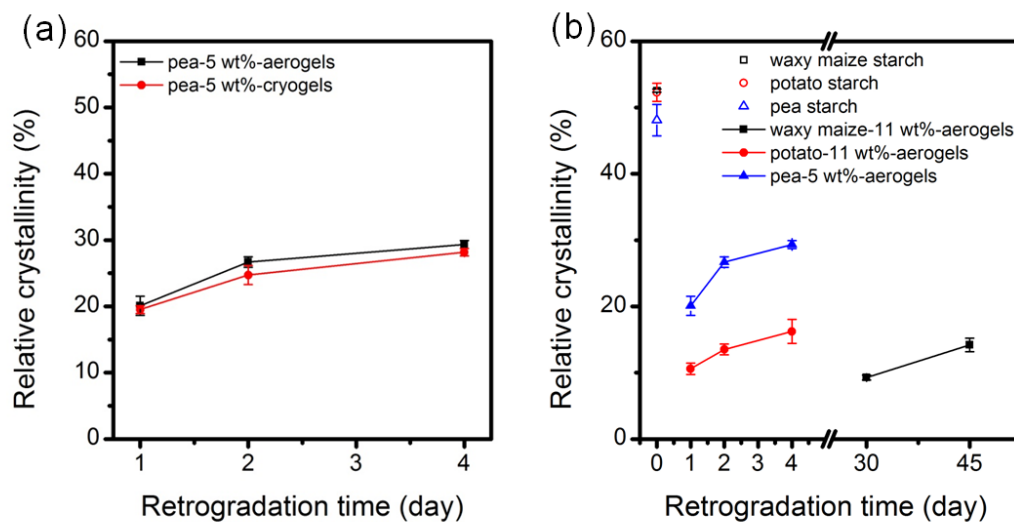
202

### 203 3. Results

#### 204 3.1 X-ray diffraction

205 An example of the relative crystallinity of starch aerogels and cryogels as a function of retrogradation  
206 time is shown in Figure 1a for pea starch aerogels and cryogels, and in Figures S1b and S1c (Supporting  
207 Information) for other starches. The examples of the diffraction profiles are shown in Figure S1a of the  
208 Supporting Information; sharp peaks on XRD profiles of the initial starches become much weaker and  
209 broader after dissolution-retrogradation, as expected (Shi & Gao, 2016; Soest, Tournois, Wit, &  
210 Vliegthart, 1995; Cheetham & Tao, 1998; Zhang, Hou, Liu, Wang, & Dong, 2019). As a consequence,  
211 the crystallinity of the initial starch significantly decreases after the dissolution-retrogradation-drying for  
212 all starches studied (Figure 1b). The decrease of the crystallinity of starch in wheat starch aerogels as  
213 compared to the initial starch have been reported previously (Ubeyitogullari et al., 2016). Figure 1a  
214 shows that drying method does not influence the crystallinity of pea starch; the same result was

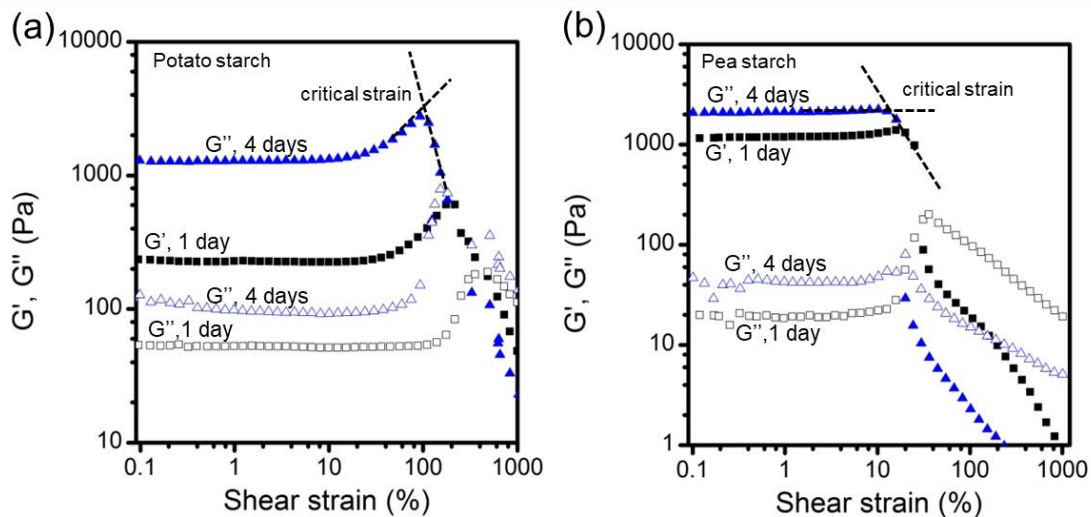
215 observed for potato and waxy maize starch (Figure S1b and S1c, respectively), and also for cellulose  
 216 aerogels and cryogels (Buchtova, Pradille, Bouvard, & Budtova, 2019). The crystallinity of aerogels  
 217 slightly increases with the increase of retrogradation time for all starches (Figure 1b), and it is the highest  
 218 for pea starch which contains the highest amount of amylose. The latter is known for much faster  
 219 crystallization than amylopectin (Ma, Ma, Zhou, Li, & Hu, 2019; Shi et al., 2016).  
 220



221  
 222 **Figure 1.** Relative crystallinity as a function of retrogradation time for (a) pea starch aerogel and  
 223 cryogel and (b) aerogels from all three types and initial starches (retrogradation time 0). Lines are  
 224 given to guide the eye. When standard deviation is not visible, it is smaller than the size of the symbol.  
 225

### 226 3.2 Rheological properties of starch gels

227 The examples of the dependences of storage and loss moduli on shear strain for potato and pea  
 228 starch gels are presented in Figure 2. For all gels the elastic behavior dominates the viscous one, as  
 229 expected, as potato and pea starch solutions are retrograded. For potato gels both moduli remain  
 230 constant within the wide strain interval: at high strains, around 100%, these gels first show strain  
 231 hardening and then break (Figure 2a). No strain hardening was observed for pea starch gels (Figure  
 232 2b).  
 233

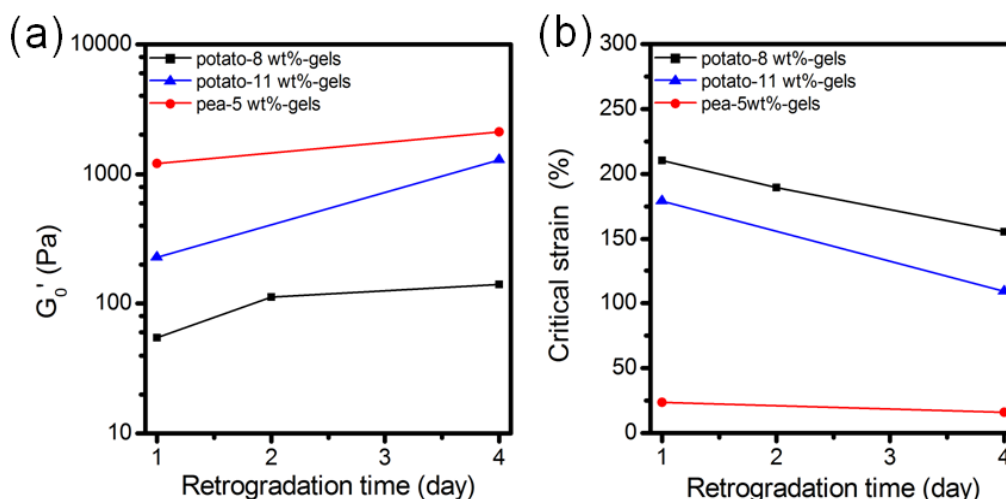


234

235 **Figure 2.** Representative dependences of storage modulus ( $G'$ , filled points) and loss modulus ( $G''$ ,  
 236 open points) as a function of shear strain at different retrogradation times for (a) potato-11wt%-gels  
 237 and (b) pea-5wt%-gels. Dashed lines are showing the determination of the critical strain.

238

239 The storage modulus in the linear region,  $G_0'$ , is plotted vs. retrogradation time in Figure 3a for all  
 240 starch gels. Higher starch concentration, denser the network and thus higher  $G_0'$ , as expected. For  
 241 example, for potato starch gels retrograded for 4 days the  $G_0'$  value increases from 141 Pa to 1290 Pa  
 242 for starch concentration varying from 8 wt% to 11 wt% (Figure 3a). The increase of retrogradation time  
 243 also leads to  $G_0'$  increase for both types of starches. Interestingly,  $G_0'$  of 5 wt% pea starch gels is higher  
 244 than that of potato starch gels of even higher concentrations, 8 wt% and 11 wt% (Figure 3a). The reason  
 245 is that pea starch contains higher amount of amylose which is known to retrograde quicker than  
 246 amylopectin and forms more crystalline regions (Putaux, Bule, & Chanzy, 2000) as reflected by higher  
 247 relative crystallinity (Figure 1b).



248  
 249 **Figure 3.** Storage moduli  $G'_0$  (a) and critical strain (b) of pea and potato starch gels as a function of  
 250 retrogradation time. Lines are given to guide the eye  
 251

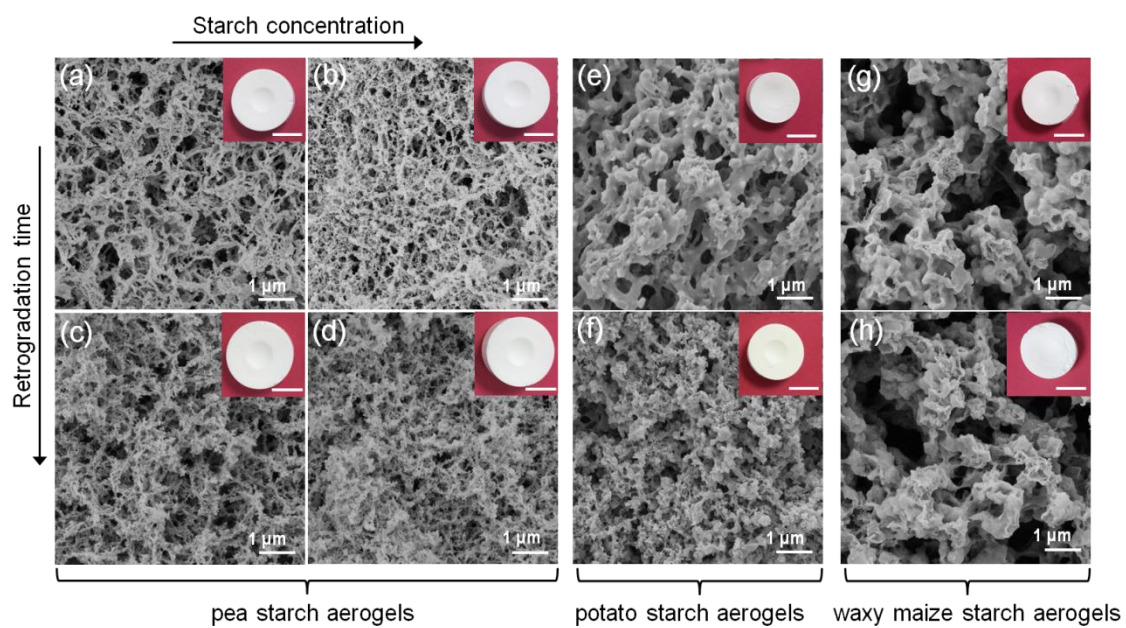
252 Critical strain is determined as the value at which gel starts to break, see details in Figure 2a and b.  
 253 The critical strain is plotted vs. retrogradation time in Figure 3b for the studied starch gels. Opposite to  
 254 the storage modulus  $G'_0$ , critical strain decreases with increasing retrogradation time and starch  
 255 concentration indicating that gels become more brittle. The most brittle are pea starch gels. Overall, the  
 256 mechanical properties of starch gels correlate well with relative crystallinity data: the higher amylose  
 257 content and longer retrogradation time, the higher is relative crystallinity and the stronger and more  
 258 brittle are starch gels.

259  
 260 **3.3 Starch aerogels: morphology and properties**

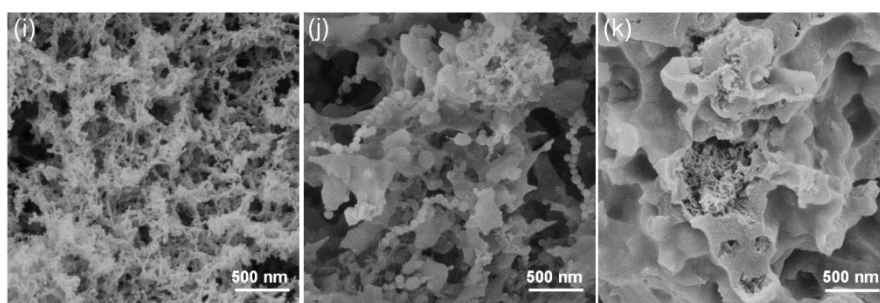
261 The examples of the inner morphology of starch aerogels is shown in Figure 4 (a-h for lower  
 262 magnification and i-k for higher magnification) for starches of different concentrations and retrograded  
 263 at different times. More examples are presented in Figure S2 and S3 of the Supporting Information.  
 264 Starch type has a significant influence on aerogel morphology: higher amylose content  
 265 (pea>potato>waxy maize), finer and more ramified is aerogel structure. Waxy maize starch aerogels  
 266 consist of rather smooth beads assembled together. Waxy maize starch solutions are retrograding very  
 267 slowly as they are based on amylopectin and even at long retrogradation times the gels are very weak.  
 268 We hypothesize that when these weak gels are placed in a non-solvent (ethanol), phase separation  
 269 occurs according to spinodal decomposition mechanism, which is also the case when cellulose is

270 coagulated in a non-solvent directly from solutions resulting in aerogels with morphology represented  
 271 by assembled together “hairy” beads (Buchtová & Budtova, 2016; Pircher et al., 2016; Sescousse,  
 272 Gavillon, & Budtova, 2011). Interestingly, the surface of the beads in the internal structure of waxy maize  
 273 aerogels is smooth but it seems that inside they are porous (Figure 4k). However, this porosity is  
 274 observable in the fracture zones only where aerogel was broken for SEM observations. Potato starch  
 275 aerogels contain a “mixture” of smooth beads and fine network while pea starch aerogels’ morphology  
 276 is represented by a fine network. The strength of a starch gel before the sample is placed in a non-  
 277 solvent plays an important role in structure formation: stronger is the gel (case of pea starch), better it  
 278 is keeping the ramified network structure. In weak gels (case of waxy maize starch) amylopectin chains  
 279 have more freedom to move, they form polymer rich phases upon the addition of non-solvent and  
 280 undergo phase separation driven by spinodal decomposition.

281



282



283

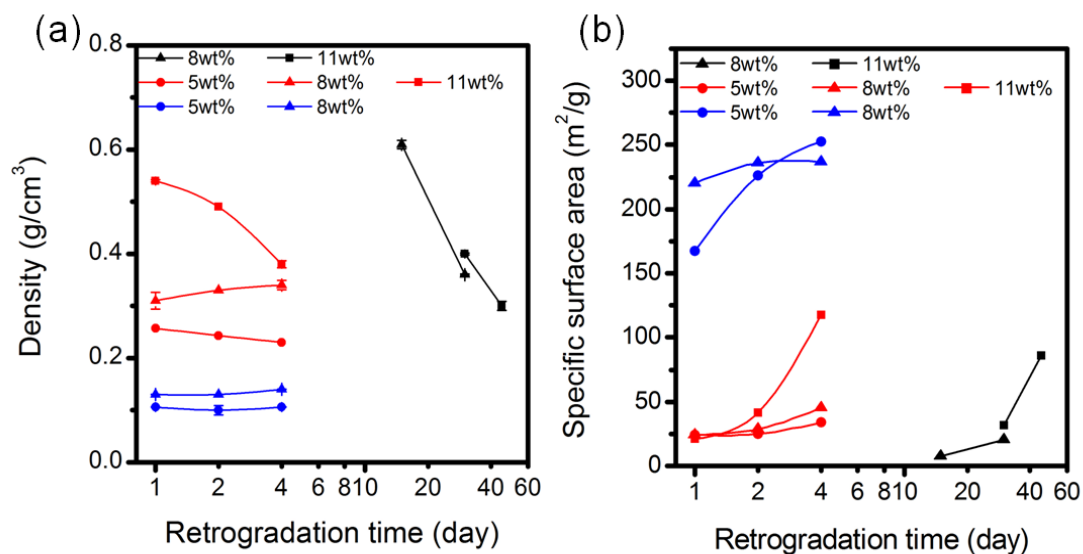
284

285 **Figure 4.** SEM images of aerogels internal morphology, insets are the digital photos of aerogel  
286 samples: (a) pea-5wt%-1day-aerogel, (b) pea-8wt%-1day-aerogel, (c) pea-5wt%-4day-aerogel, (d)  
287 pea-8wt%-4day-aerogel, (e) potato-11wt%-1day-aerogel, (f) potato-11wt%-4day-aerogel, (g) waxy  
288 maize-11wt%-30day-aerogel, (h) waxy maize-11wt%-45day-aerogel, (i) pea-8wt%-4day-aerogel, (j)  
289 potato-8wt%-4day-aerogel and (k) waxy maize-8wt%-15day-aerogel. The scale bars for photos of  
290 aerogels are 1 cm.

291

292 Higher starch concentration leads to denser network morphology (see Figure 4 for pea starch  
293 aerogels), the same was observed for other bio-aerogels (Buchtová et al, 2016; Groult et al, 2018b).  
294 Longer retrogradation times induce more ramified structure for amylose-containing starches (Figure 4).

295 Aerogel density and specific surface area are summarized in Fig. 5, and linear shrinkage (eq.1) and  
296 porosity (eq. 2) in Figure S4. Pea starch aerogels possess the lowest shrinkage, lowest density and  
297 highest porosity at all concentrations and retrogradation times: higher amylose content in starch leads  
298 to quicker retrogradation, highest relative crystallinity (Figure 1) and strongest gels (Figure 3a), helping  
299 to “resist” solvent exchange and drying. Higher starch concentration, lower shrinkage, as higher polymer  
300 concentration also leads to stronger gels. The same phenomenon was observed for cellulose and pectin  
301 aerogels (Buchtová et al, 2016; Groult et al, 2018b). Despite lower shrinkage with the increase of starch  
302 concentration, density increases (García-González et al., 2013; Ubeyitogullari et al., 2016) and porosity  
303 decreases, which shows that added matter “dominates” small gain in volume (Figure 5a and S4b). A  
304 strong influence of retrogradation time on shrinkage (Figure S4a), density (Figure 5a) and porosity  
305 (Figure S4b) is recorded for waxy maize aerogels as even retrograded for a long time (15 days) the gels  
306 are very weak and contract under solvent exchange and drying, as in the case of non-gelled pectin  
307 solutions (Groult et al., 2018b).



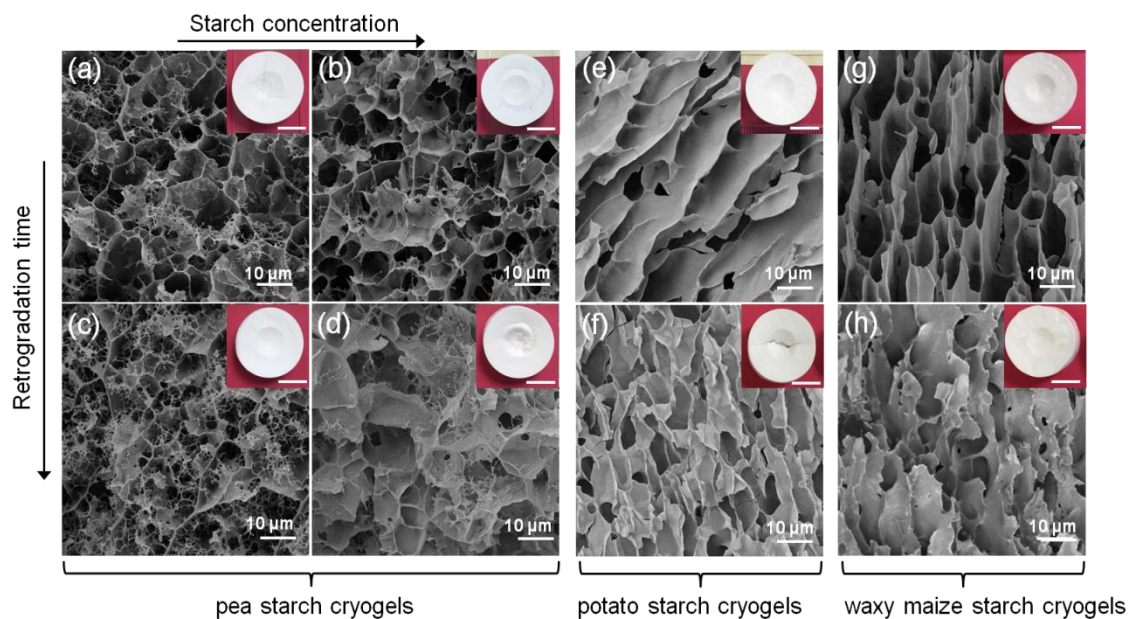
308  
 309 **Figure 5.** Density (a) and specific surface area (b) of starch aerogels from different starch sources and  
 310 concentrations as a function of retrogradation time. Black, red, and blue data points correspond to  
 311 waxy maize, potato and pea starch aerogels, respectively. Lines are given to guide the eye. If  
 312 standard deviations for density values are not visible, they are within the dimension of the symbol.

313  
 314 Pea starch aerogels show the highest specific surface area among all aerogels studied, from around  
 315 160 - 250 m<sup>2</sup>/g vs 8 - 120 m<sup>2</sup>/g for potato and waxy maize aerogels (Figure 5b). Fine and ramified  
 316 morphology of pea starch aerogels is the reason of higher specific surface area, see Figure 4. Specific  
 317 surface area increases with the increase of starch concentration and of retrogradation time (Figure 5b).  
 318 For cellulose aerogels it was suggested that higher polymer concentration leads to the “division” of  
 319 pores into smaller ones thus increasing specific surface area (Buchtová et al., 2016); the same can also  
 320 be assumed for starch aerogels. Network ramification with retrogradation time shown by SEM (Figure  
 321 4) confirms the increase of specific surface area.

322  
 323 3.4 Starch cryogels: morphology and properties

324 The morphology of starch cryogels is shown in Figure 6, more SEM images for potato and waxy  
 325 maize starch cryogels can be found in Figures S5 and S6, respectively. All cryogels have very large  
 326 macropores which are the replica of ice crystals that grew under freezing and “pushed aside” pore walls  
 327 of starch gel. The pore sizes, as seen from SEM images, are smaller (especially for pea cryogels) than  
 328 those reported in literature for the cases of freeze-dried amylopectin (7 days retrogradation) or non-

329 retrograded potato and corn starch solutions (Nakamatsu et al., 2006; Svagan et al., 2008). As all our  
 330 samples were prepared in the same freezing and lyophilization conditions, it is the intrinsic properties of  
 331 the starch that influence cryogel morphology. Stronger are the gels, better they “resist” to the growth of  
 332 ice crystals. The pores in the retrograded pea starch aerogels do not show any preferential orientation  
 333 despite unidirectional freezing; potato starch gels are weaker than pea starch and pores become  
 334 oriented, and the weakest gels are those based on waxy maize starch and pores are strongly oriented  
 335 in the direction of the growth of ice crystals as in the case of nanocellulose (Chau et al., 2016). Waxy  
 336 maize starch is thus suitable for ice templating method. Potato and waxy maize starch cryogels have  
 337 smooth pore walls, as in the case of amylopectin freeze-dried starch (Svagan et al., 2008), while those  
 338 of pea starch are thinner and the network is more ramified. Pores with smooth walls and no preferential  
 339 orientation were observed for cellulose cryogels made via unidirectional or isotropic freeze drying  
 340 (Buchtová et al., 2016). In that case the structure of the network of cellulose coagulated in water resisted  
 341 the unidirectional growth of ice crystals but resulted in smooth and thick pore walls and pore’s size  
 342 smaller than in starch cryogels.  
 343



344  
 345 **Figure 6.** SEM images of cryogels' internal morphology, the insets show the digital photos of cryogels:  
 346 (a) pea-5wt%-1day-cryogel, (b) pea-8wt%-1day-cryogel, (c) pea-5wt%-4day-cryogel, (d) pea-8wt%-  
 347 4day-cryogel, (e) potato-8wt%-1day-cryogel, (f) potato-8wt%-4day-cryogel, (g) waxy mazie-8wt%-  
 348 30day-cryogel and (h) waxy mazie-8wt%-45day-cryogel. The scale bars for photos of cryogels are 1  
 349 cm.

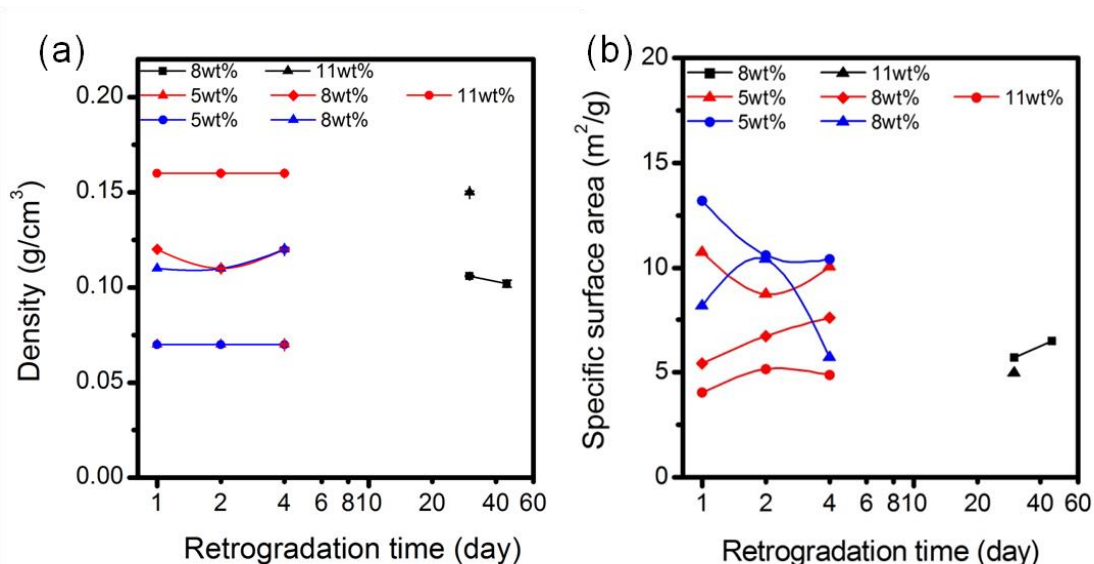


350

351 The increase of starch concentration seems to slightly decrease pore sizes of cryogels (Figures 6,  
352 S5 and S6), however, it is retrogradation time which impacts starch cryogel morphology: the longer  
353 retrogradation, the smaller the pores for all types of starches used in this work. The same was observed  
354 for all starch aerogels and is the sign of starch network ramification during retrogradation.

355 The density, porosity and specific surface area of all starch cryogels are summarized in Figure 7 and  
356 S4c as a function of retrogradation time. Practically no shrinkage was observed as no solvent/non-  
357 solvent exchange was performed for the preparation of cryogels. All cryogels have very low density,  
358 lower than that of aerogels, 0.07 - 0.16 vs 0.1 - 0.6 g/cm<sup>3</sup>; a similar trend was reported for cellulose  
359 aerogels and cryogels (Buchtová et al., 2016). Higher starch concentration led to higher cryogel density  
360 and lower porosity, as expected, and no influence of retrogradation time was observed (Figure 7a).

361



362  
363 **Figure 7.** (a) Density and (b) specific surface area of cryogels from starch different concentrations and  
364 sources as a function of retrogradation time. Black, red, and blue data points correspond to waxy  
365 maize, potato, and pea starch cryogels, respectively. The lines are given to guide the eye. When  
366 standard deviations for density values are not seen, they are within the dimensions of the symbol.

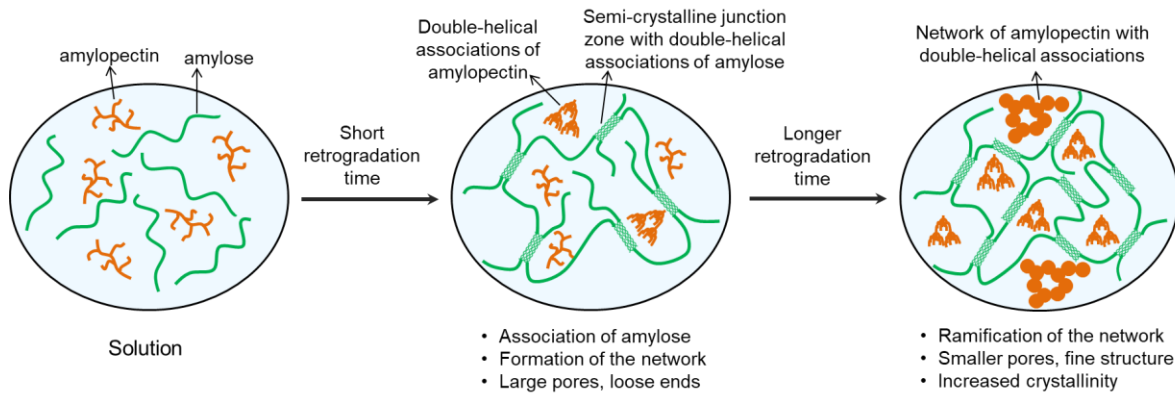
367  
368 The specific surface area of all cryogels (Figure 7b) is very low, within 3 - 13 m<sup>2</sup>/g, which is at least  
369 20-30 times lower than that of aerogels (see Figure 5b). We consider all values obtained for cryogels  
370 being similar within experimental errors which is around 10 m<sup>2</sup>/g. Thus, no trend can be deduced.

371

#### 372 **4. Discussion**

373 Based on all results obtained, we propose the following structure evolution in starch gels resulting in  
374 different aerogel morphology and properties. It is known that during retrogradation amylose associates  
375 into parallel double helices connected by amorphous regions, the whole forms semi-crystalline clusters  
376 (Putaux et al., 2000). We assume that at the early stages of retrogradation, amylose network with large  
377 pores, loose ends and junctions based of semi-crystalline clusters is formed (Figure 8); these gels are  
378 weak. At this stage, amylopectin starts to slowly associate to form necklace-like nano-structures (Putaux  
379 et al., 2000). With the increase of retrogradation time the crystallinity increases and gel becomes  
380 stronger: amylose chains, if present, form more and more junction zones leading to network  
381 reinforcement and ramification, the latter inducing the increase of specific surface area of aerogels. For  
382 the neat amylopectin solutions, it was shown that amylopectin forms a fractal network built of necklace-  
383 like structures (Putaux et al., 2000). We suppose that these nano-structures are too weak to resist  
384 solvent/non-solvent exchange: they collapse into much larger entities according to spinodal phase  
385 separation mechanism. We also hypothesize that with the increase of retrogradation time, amylose does  
386 not form longer and/or thicker “zip”-type structures which would lead to the decrease of specific surface  
387 area of aerogels. We assume that it is larger number of crystalline junctions that are formed with longer  
388 retrogradation resulting in stronger gels with higher crystallinity and more ramified network, the latter  
389 reflected by the increase of aerogels specific surface area (Figure 8). Higher amylose content in pea  
390 starch amplifies this phenomenon. It may also be possible that the presence of amylopectin in pea and  
391 potato starches prevents amylose condensing into thick aggregates, as was found for amylose alone in  
392 (Putaux et al., 2000), thus helping network ramification. As at higher amylose content gels are stronger,  
393 the shrinkage during aerogels' preparation is lower and the density of aerogels is also lower as  
394 compared to that of low-amylose content starch aerogels. The influence of amylose content of aerogel  
395 and cryogel density and on aerogel specific surface area is summarized in Figure 9.

396



397

398

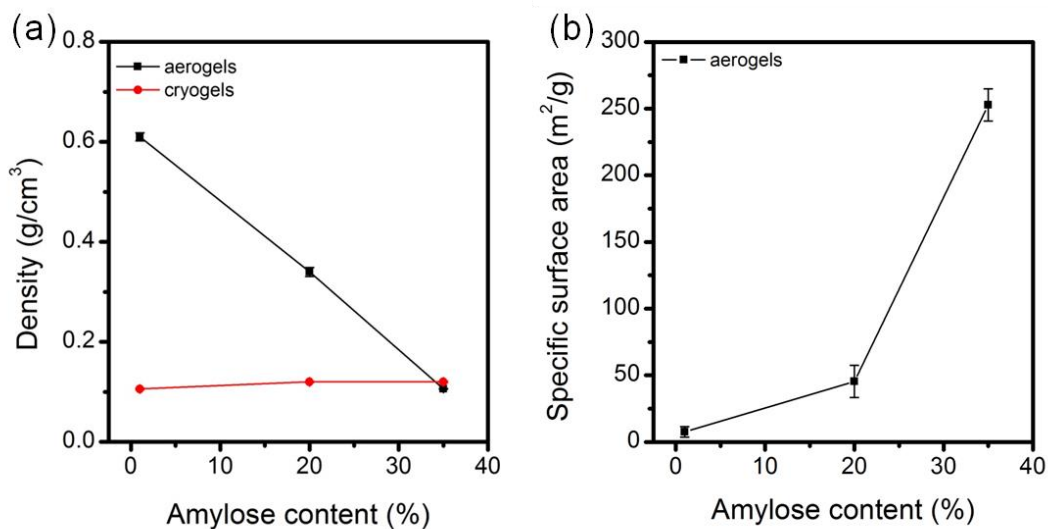
**Figure 8.** A schematic presentation of structure evolution in starch gels with the increase of

399

retrogradation time.

400

401



402

403

**Figure 9.** Density (a) and specific surface area (b) of starch aerogels and cryogels from 8 wt%

404

solutions as a function of amylose content. The retrogradation time is 4 days for pea and potato

405

starches and 15 days for waxy maize. The lines are given to guide the eye. When standard deviations

406

values are not seen, they are within the dimensions of the symbol.

407

408

In the view of the said above, a schematic presentation summarizing structure evolution in all

409

samples studied as a function of amylose content, starch concentration and retrogradation time is

410

presented in Figure 10. In all the cases, with the increase of starch concentration and retrogradation

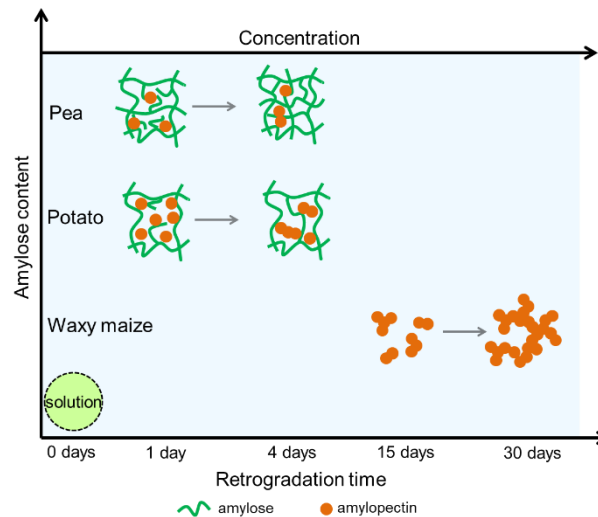
411

time, the specific surface area of aerogels increases as the network becomes more ramified. Pea starch

412

aerogels with the highest amylose content (33–36%) possess the highest specific surface area due to

413 the finest morphology amylose network (see Figure 9b). As pea starch gels are the strongest, their  
 414 density is the lowest (Figure 9a). Potato aerogels with 18-21% of amylose present a mixed morphology  
 415 of amylopectin beads and amylose network. Their specific surface area is lower than that of pea starch  
 416 aerogels, and as the gels are weaker, the density is higher due to stronger shrinkage (Figure 9a). Waxy  
 417 maize starch aerogels with only 1 % of amylose have the largest pores with the lowest specific surface  
 418 area and the highest density (Figure 9).



419  
 420 **Figure 10.** A schematic presentation summarizing structure evolutions in all starch samples, as  
 421 deduced from aerogel morphology and properties, as a function of amylose content, starch  
 422 concentration and retrogradation time. “0 days” correspond to the initial solution.

423  
 424 Various morphologies obtained in porous starches are interesting for different biomedical applications,  
 425 in particular as no toxic compounds were used. For example, larger pores are suitable for making  
 426 scaffolds for cells growth, and smaller pores are attractive for control release applications.

427  
 428 **5. Conclusions**

429 Highly porous starch materials were made from starch gels using two ways of drying: with  
 430 supercritical CO<sub>2</sub> and freeze-drying. The influence of starch type (amylose content) and process  
 431 parameters (starch concentration and retrogradation time) on the morphology, density and specific  
 432 surface area were systematically studied and correlated with relative crystallinity and gel strength.

433 Drying mode had a significant impact on the properties of the dry material: freeze-dried starch gels  
 434 had lower density and much lower specific surface area as compared to those of aerogels. This was an

435 expected result as the morphology and properties of materials freeze-dried from water are dominated  
436 by the growth of ice crystals. Relative crystallinity dropped significantly after starch dissolution-  
437 retrogradation-drying but was not influenced by the drying mode.

438 As drying with supercritical CO<sub>2</sub> is well preserving the morphology of starch gels, amylose content  
439 and retrogradation time were playing an important role in the understanding of aerogel properties. Higher  
440 amylose content, higher relative crystallinity and gel strength, lower sample shrinkage and lower aerogel  
441 density. Different ways of amylose and amylopectin chains reorganization during retrogradation and  
442 their different gelation kinetics is evidenced by the evolution of aerogel specific surface area: pea starch  
443 aerogels possess the highest surface area, followed by potato and then by waxy maize starch. With  
444 retrogradation, amylose forms more and more fine network leading to the increase of aerogel surface  
445 area. At very long retrogradation times amylopectin (waxy maize starch) is also gelling, but the gels are  
446 weak and shrinking during processing, resulting in higher density and lower specific surface area.

447 The results obtained offer a new way of investigation of starch gels properties using drying with  
448 supercritical CO<sub>2</sub>. Opposite to freeze-dried starch, aerogels reflect the structure and its evolution in  
449 starch gels; this mode of drying can thus be used as a tool for a deeper understanding of the structure  
450 and properties of starch gels.

451

## 452 **Acknowledgments**

453 Authors are grateful to Roquette for sponsoring the work and providing starches, to Pierre Ilbizian  
454 (PERSEE, MINES ParisTech) for the supercritical CO<sub>2</sub> drying, to Suzanne Jacomet (CEMEF, MINES  
455 ParisTech) for the help with SEM and to Gabriel Monge (CEMEF, MINES ParisTech) for performing  
456 XRD.

457

458

459

460

461 **References**

- 462 Buchtová, N., & Budtova, T. (2016). Cellulose aero-, cryo- and xerogels: towards understanding of  
463 morphology control. *Cellulose*, 23, 2585-2595.
- 464 Buchtova, N., Pradille, C., Bouvard, J. L., & Budtova, T. (2019). Mechanical properties of cellulose  
465 aerogels and cryogels. *Soft Matter*, 15, 7901-7908.
- 466 Budtova, T. (2019). Cellulose II aerogels: a review. *Cellulose*, 26, 81-121.
- 467 Chau, M., De France, K. J., Kopera, B., Machado, V. R., Rosenfeldt, S., Reyes, L., et al. (2016). Composite  
468 Hydrogels with Tunable Anisotropic Morphologies and Mechanical Properties. *Chemistry of*  
469 *Materials*, 28, 3406-3415.
- 470 Cheetham W.H. N., & Tao, L. (1998). Variation in Crystalline Type with Amylose Content in Maize  
471 Starch Granules An X-Ray Powder Diffraction Study. *Carbohydrate Polymers*, 36, 277-284.
- 472 Druel, L., Bardl, R., Vorweg, W., & Budtova, T. (2017). Starch Aerogels: A Member of the Family of  
473 Thermal Superinsulating Materials. *Biomacromolecules*, 18, 4232-4239.
- 474 García-González, C. A., & Smirnova, I. (2013). Use of supercritical fluid technology for the production  
475 of tailor-made aerogel particles for delivery systems. *The Journal of Supercritical Fluids*, 79,  
476 152-158.
- 477 García-González, C. A., Uy, J. J., Alnaief, M., & Smirnova, I. (2012). Preparation of tailor-made starch-  
478 based aerogel microspheres by the emulsion-gelation method. *Carbohydrate Polymers*, 88,  
479 1378-1386.
- 480 Glenn, G. M., & Irving, D. W. (1995) Starch-Based Microcellular Foams. *Cereal Chemistry*, 72, 155-161.
- 481 Glenn, G. M., Klamczynski, A., Chiou, B. S., Orts, W. J., Imam, S. H., & Wood, D. F. (2008). Temperature  
482 Related Structural Changes in Wheat and Corn Starch Granules and Their Effects on Gels and  
483 Dry Foam. *Starch - Stärke*, 60, 476-484.
- 484 Grout, S., & Budtova, T. (2018a). Thermal conductivity/structure correlations in thermal super-  
485 insulating pectin aerogels. *Carbohydrate Polymers*, 196, 73-81.

486 Groult, S., & Budtova, T. (2018b). Tuning structure and properties of pectin aerogels. *European Polymer*  
487 *Journal*, 108, 250-261.

488 Hamed, M., Karabulut, E., Marais, A., Herland, A., Nystrom, G., & Wagberg, L. (2013). Nanocellulose  
489 aerogels functionalized by rapid layer-by-layer assembly for high charge storage and beyond.  
490 *Angewandte Chemie. International Ed. In English*, 52, 12038-12042.

491 Himmel, B., Gerber, T., Biirger, H., Holzfiter, G., & Olbertz, A. (1995). Structural characterization of  
492  $\text{SiO}_2\text{-Al}_2\text{O}_3$  aerogels. *Journal of Non-Crystalline Solids*, 186, 149-158.

493 Kistler, S. S. (1931). Coherent expanded aerogels and gellies. *Nature*, 127, 741.

494 Komiya, T., & Nara, S. (1986). Changes in Crystallinity and Gelatinization Phenomena of Potato Starch  
495 by Acid Treatment. *Starch-Starke*, 38, 9-13.

496 Korhonen, O., & Budtova, T. (2020). All-cellulose composite aerogels and cryogels. *Composites Part A:*  
497 *Applied Science and Manufacturing*, 137, 106027

498 Lavoine, N., & Bergström, L. (2017). Nanocellulose-based foams and aerogels: processing, properties,  
499 and applications. *Journal of Materials Chemistry A*, 5, 16105-16117.

500 Ma, Z., Ma, M., Zhou, D., Li, X., & Hu, X. (2019). The retrogradation characteristics of pullulanase  
501 debranched field pea starch: Effects of storage time and temperature. *International Journal of*  
502 *Biological Macromolecules*, 134, 984-992.

503 Mallepally, R. R., Bernard, I., Marin, M. A., Ward, K. R., & McHugh, M. A. (2013). Superabsorbent  
504 alginate aerogels. *The Journal of Supercritical Fluids*, 79, 202-208.

505 Mehling, T., Smirnova, I., Guenther, U., & Neubert, R. H. H. (2009). Polysaccharide-based aerogels as  
506 drug carriers. *Journal of Non-Crystalline Solids*, 355, 2472-2479.

507 Nakamatsu, J., Torres, F. G., Troncoso, O. P., Min-Lin, Y., & Boccaccini, A. R. (2006). Processing and  
508 Characterization of Porous Structures from Chitosan and Starch for Tissue Engineering  
509 Scaffolds. *Biomacromolecules*, 7, 3345-3355.

510 Pierre A. C. (2011). History of aerogels. In M. A. Aegerter et al (Eds), *Aerogels handbook, advances in*  
511 *sol-gel derived materials and technologies* (pp. 813–831). Springer, New York

512 Pircher, N., Carbajal, L., Schimper, C., Bacher, M., Rennhofer, H., Nedelec, J. M., et al. (2016). Impact  
513 of selected solvent systems on the pore and solid structure of cellulose aerogels. *Cellulose*  
514 *(Lond)*, 23, 1949-1966.

515 Putaux, J. L., Bule, A., & Chanzy, H. (2000). Network Formation in Dilute Amylose and Amylopectin  
516 Studied by TEM. *Macromolecules*, 33, 6416-6422.

517 Robitzer, M., David, L., Rochas, C., Renzo, F. D., & Quignard, F. (2008). Nanostructure of Calcium  
518 Alginate Aerogels Obtained from Multistep Solvent Exchange Route. *Langmuir*, 24, 12547-  
519 12552.

520 Rooke, J., Passos, C. M., Chatenet, M., Sescousse, R., Budtova, T., Berthon-Fabry, S., et al. (2011).  
521 Synthesis and Properties of Platinum Nanocatalyst Supported on Cellulose-Based Carbon  
522 Aerogel for Applications in PEMFCs. *Journal of the Electrochemical Society*, 158, B779-B789.

523 Sai, H., Fu, R., Xing, L., Xiang, J., Li, Z., Li, F., et al. (2015). Surface modification of bacterial cellulose  
524 aerogels' web-like skeleton for oil/water separation. *ACS Appl Mater Interfaces*, 7, 7373-7381.

525 Saliger, R., Heinrich, T., Gleissner, T., & Fricke, J. (1995). Sintering behaviour of alumina-modified silica  
526 aerogels. *Journal of Non-Crystalline Solids*, 186, 113-117.

527 Sescousse, R., Gavillon, R., & Budtova, T. (2011). Aerocellulose from cellulose–ionic liquid solutions:  
528 Preparation, properties and comparison with cellulose–NaOH and cellulose–NMMO routes.  
529 *Carbohydrate Polymers*, 83, 1766-1774.

530 Shi, M., & Gao, Q. (2016). Recrystallization and in vitro digestibility of wrinkled pea starch gel by  
531 temperature cycling. *Food Hydrocolloids*, 61, 712-719.

532 Silva, E. K., Azevedo, V. M., Cunha, R. L., Hubinger, M. D., & Meireles, M. A. A. (2016). Ultrasound-  
533 assisted encapsulation of annatto seed oil: Whey protein isolate versus modified starch. *Food*  
534 *Hydrocolloids*, 56, 71-83.

535 Soest, J. J. G. V., Tournois, H., Wit, D. D., & Vliegthart, J. F. G. (1995). Short-Range Structure in  
536 (Partially) Crystalline Potato Starch Determined with Attenuated Total Reflectance Fourier-  
537 Transform IR Spectroscopy. *Carbohydrate Research*, 279, 201-214.



538 Spada, J. C., Norena, C. P., Marczak, L. D., & Tessaro, I. C. (2012). Study on the stability of beta-carotene  
539 microencapsulated with pinhao (*Araucaria angustifolia* seeds) starch. *Carbohydrate Polymers*,  
540 89, 1166-1173.

541 Svagan, A. J., Samir, M. A. S. A., & Berglund, L. A. (2008). Biomimetic Foams of High Mechanical  
542 Performance Based on Nanostructured Cell Walls Reinforced by Native Cellulose Nanofibrils.  
543 *Advanced Materials*, 20, 1263-1269.

544 Ubeyitogullari, A., & Ciftci, O. N. (2016). Formation of nanoporous aerogels from wheat starch.  
545 *Carbohydrate Polymers*, 147, 125-132.

546 Ulker, Z., & Erkey, C. (2014). An emerging platform for drug delivery: aerogel based systems. *Journal*  
547 *of Controlled Release*, 177, 51-63.

548 Zhang, B., Wang, K., Hasjim, J., Li, E., Flanagan, B. M., Gidley, M. J., et al. (2014). Freeze-drying changes  
549 the structure and digestibility of B-polymorphic starches. *Journal of Agricultural and Food*  
550 *Chemistry*, 62, 1482-1491.

551 Zhang, H., Hou, H., Liu, P., Wang, W., & Dong, H. (2019). Effects of acid hydrolysis on the  
552 physicochemical properties of pea starch and its film forming capacity. *Food Hydrocolloids*, 87,  
553 173-179.

554 Zhao, H. B., Chen, M., & Chen, H. B. (2017). Thermally Insulating and Flame-Retardant  
555 Polyaniline/Pectin Aerogels. *ACS Sustainable Chemistry & Engineering*, 5, 7012-7019.

556 Zhu, F. (2019). Starch based aerogels: Production, properties and applications. *Trends in Food Science*  
557 *& Technology*, 89, 1-10.

558 Zou, F., Peng, L., Fu, W., Zhang, J., & Li, Z. (2015). Flexible superhydrophobic polysiloxane aerogels for  
559 oil–water separation via one-pot synthesis in supercritical CO<sub>2</sub>. *RSC Advances*, 5, 76346-76351.

560 Zou, F., Yue, P., Zheng, X., Tang, D., Fu, W., & Li, Z. (2016). Robust and superhydrophobic thiourethane  
561 bridged polysilsesquioxane aerogels as potential thermal insulation materials. *Journal of*  
562 *Materials Chemistry A*, 4, 10801-10805.